Energy Equip. Sys./ Vol. 8/No. 1/March 2020/ 55-80

ENERGY EQUIPSYS

Energy Equipment and Systems

http://energyequipsys.ut.ac.ir
www.energyequipsys.com

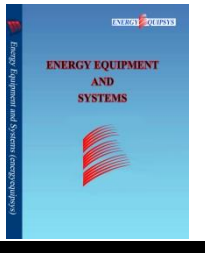

Unsteady aerodynamic performance of Dual-Row H-Darrieus vertical axis wind turbine

Authors

Mojtaba Tahani [a]
Mohsen Razavi [a]
Mojtaba Mirhosseini [b*]
Fatemeh Razi Astaraei [a]
Saeede Mirmahdian [a]

[a] Faculty of New Sciences and Technologies, University of Tehran, Tehran, Iran

[b] Department of Energy Technology, Aalborg University, Pontoppidanstraede 111, 9220 Aalborg East, Denmark

Article history:

Received : 8 May 2019
Accepted : 3 November 2019

ABSTRACT

H-rotor Vertical Axis Wind Turbine (VAWT) is one of the most efficient energy suppliers which have been investigated in many recent types of research. The aim of this work is to study the aerodynamic performance of a doubled-row H-Darrieus VAWT. First, an ordinary three-bladed VAWT with NACA4415 profile is simulated by means of 3D computational fluid dynamics (CFD) and results are compared to a recently published research work based on Blade Element Momentum (BEM) theory. Afterward, a doubled-row H-Darrieus VAWT is simulated and analyzed in two different geometric configurations. In the first configuration, a second row with the same blade characteristics of the first row is added aligned with the first row and with 0.2 m distance toward it. In the second one, again with the same blade characteristics, the secondary blade is added with 0.2 m distance toward first row, but with 60 degrees angular offset. Renormalization-Group (RNG) k-ε turbulence model besides wall function is applied in all unsteady simulations. As comparative tools, based on other studies using the same coefficients, momentum coefficient (C_m) and power coefficient (C_p) are calculated in all simulations to investigate which case operates more efficiently. It is observed that adding a second row to an ordinary H-Darrieus VAWT will improve these coefficients up to 314% which is a considerable leap in power production ability of the VAWT. Also, different turbulence models, geometries (with a central shaft and without central shaft) and solution methods were also analyzed and the effect of each one was computed and compared with other cases.

Keywords: H-Darrieus; Doubled-Row VAWT; BEM; CFD; Performance.

1. Introduction

Energy has been the main concern of human life during recent years. This is not only about how much energy we need, but also there are several other criteria that affect energy supply like influence on the environment and amount of fossil fuel used. These two mentioned points; meaning the amount of energy needed and consideration of environmental effects have forced researchers to switch from traditional ways of energy supply to new and renewable ones. Meanwhile, wind energy, as a renewable form of energy, has not been outside of researchers' scope. In order to optimize energy supply from wind, efforts have been done to improve the performance of both horizontal and vertical axis wind turbines. In this study the focus is on VAWTs.

Many analytical models such as Stream Tube (ST), Multiple Stream Tube (MST), and Double Multiple Stream Tube (DMST) etc. have been introduced to optimize vertical axis wind turbines alongside with CFD analysis.

* Corresponding author: Mojtaba Mirhosseini
Department of Energy Technology, Aalborg University, Pontoppidanstraede 111, 9220 Aalborg East, Denmark
Email: seh@et.aau.dk

Paraschivoiu [1] introduced DMST as one of the most perfect models for analyzing VAWTs. By dividing the general stream tube into upwind, downwind and longitudinal sections, DMST model resulted in more accurate outputs in comparison with previous models. Abu-El-Yazied et al. [2] studied the effect of adding a barrier to an ordinary Darrieus VAWT. These barriers were to prevent negative torque and also to increase the velocity of the wind entering the rotor. Results indicated impressive performance improvement by using barriers. El Baz et al. [3] used CFD analysis for studying the influence of an additional airfoil when added exactly adjacent to the trailing edge of the main airfoil. 2D CFD simulations showed that this modified design will result in higher power coefficients in low speeds. The main reason for this improvement was the cancellation of negative torque at some azimuthal angles. Hamada et al. [4] examined different types of k-ε turbulence model to study dynamic stall around the blades and the interaction of blade wakes. Zhang et al. [5] used RNG k-ε to analyze the effect of grid number, computational domain, near-wall grid and time step on simulation accuracy. Chen and Lian [6] applied RNG k-ε to study vortex-blade interaction in an H-rotor VAWT. Their work resulted in significant outputs about the effect of airfoil thickness and solidity on torque and torque coefficient. Rashedul Hasan et al. [7] used CFD analysis in order to gain some vital parameters for the practical implementation of VAWTs. Lam et al. [8] used Transition Shear Stress Transport (SST) and Detached Eddy Simulation (DES) models to study the wake characteristics of a vertical axis wind turbine. Tahani et al. [9] proposed a novel heuristic method for optimizing a VAWT design. This method was a combination of continuous/discrete optimization algorithms with DMST model which was supported by means of a CFD simulation done by SST model. Wang et al. [10] introduced a novel Darrieus vertical axis wind turbine whose blade can be deformed into a desired geometry and achieve better aerodynamic performance. Lee et al. [11] used RNG k-ε to study performance and shape characteristics of a helical Savonius wind turbine at various helical angles. Li et al. [12] used RNG k-ε turbulence model to study the influence of adding a flexible, scalable auxiliary vane mechanism into the rotor of a straight-bladed VAWT. This study resulted in an increase in momentum coefficient at a low tip speed ratio. Rogowski et al. [13] used SST k-ω and RNG k-ε turbulence models to study aerodynamic loads of a Darrieus wind turbine. Scungio et al. [14] employed a wind tunnel test to investigate the effect of adding an auxiliary airfoil beside each of the main blades of a three-bladed Darrieus VAWT. It was concluded that this addition can improve the torque coefficient significantly. Saeidi et al. [15] used DMST model for introducing a site-specific 3 bladed H-Darrieus VAWT and extracting torque and power plots for different tip speed ratios. This was observed that DMST model can accurately predict the performance. Detection of this accuracy was because of a comparative study between DMST model and experimental model.

As it can be seen in many of recent researches, the geometric optimization of VAWTs has turned to be of higher importance in researchers' area of attention. In order to take further steps; in this research study, adding a second row to an ordinary H-Darrieus VAWT has been investigated. The main novelties of this effort can be prioritized as follows:

1- Addition of a second row to an ordinary H-Darrieus VAWT (in two different geometric situations) to investigate the effect of this geometric shift on the averaged value of momentum coefficient (C_m) and power coefficient (C_p) ,
2- Using CFD analysis as the main tool in order to simulate an ordinary VAWT, compare the result of this simulation with recent BEM results and investigate the effect of adding a second row to an ordinary VAWT; respectively.
3- Utilizing CFD approach in several simulations requires high levels of accuracy and efficiency. In order to maintain these two, all results are backed up by several studies comparing different turbulence models, meshing algorithms, domain dimensions, solution methods, and geometries. Also, the required solution time for each of mentioned simulations has been calculated in order to have a trade-off between accuracy and efficiency.

Figure 1 represents a schematic view of the geometry for the VAWT introduced in reference [15].

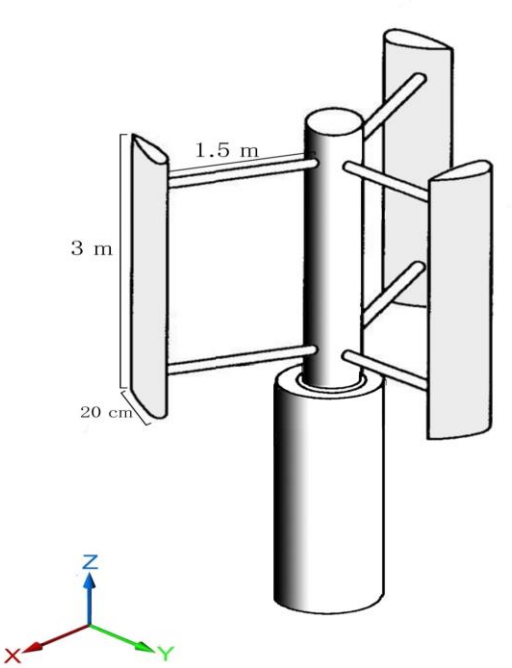

Fig.1. 3D schematic view of introduced VAWT

2. Governing Equations

In the present work, Unsteady Reynolds Averaged Navier Stokes (URANS) equations are solved for simulations. Momentum equation is written in the following form:

$$\frac{\partial \mathrm{u_i}}{\partial \mathrm{t}} + \mathrm{u_j}\frac{\partial \mathrm{u_i}}{\partial \mathrm{x_j}} = -\frac{1}{\rho}\frac{\partial \mathrm{P}}{\partial \mathrm{x_i}} - \frac{\partial}{\partial \mathrm{x_j}}\left\{\mathrm{v}\left(\frac{\partial \mathrm{u_i}}{\partial \mathrm{x_j}} + \frac{\partial \mathrm{u_j}}{\partial \mathrm{x_i}} - \frac{2}{3}\,\delta_{\mathrm{ij}}\frac{\partial \mathrm{u_l}}{\partial \mathrm{l}}\right)\right\} + \frac{\partial}{\partial \mathrm{x_j}}\left(-\overline{\acute{\mathrm{u}}_{\mathrm{i}}\acute{\mathrm{u}}_{\mathrm{j}}}\right) \quad (1)$$

Re-Normalization Group k-ε (RNG k-ε) has been chosen for simulations. Precise performance of this model toward shear flows and separation are reasons of this choice alongside with its capability for swirling flows. Also, estimation of this model for Darrieus VAWTs is accepted based on comparisons with experimental and analytical models [2],[4–7],[16–18].

Transport equations of the selected model are as follows [19]:

$$\frac{\partial}{\partial t}(\rho k) + \frac{\partial}{\partial x_i}(\rho k u_i) = \frac{\partial}{\partial x_j}\left(\alpha_k \mu_{eff}\frac{\partial k}{\partial x_j}\right) + G_k + G_b - \rho\varepsilon - Y_M + S_k \quad (2)$$

$$\frac{\partial}{\partial t}(\rho \varepsilon) + \frac{\partial}{\partial x_i}(\rho \varepsilon u_i) = \frac{\partial}{\partial x_j}\left(\alpha_\varepsilon \mu_{eff}\frac{\partial \varepsilon}{\partial x_j}\right) + C_{1\varepsilon}\frac{\varepsilon}{k}(G_k + C_{3\varepsilon}G_b) - C_{2\varepsilon}\rho\frac{\varepsilon^2}{k} - R_\varepsilon + S_\varepsilon \quad (3)$$

where G_k is the generation of turbulence kinetic energy as a result of mean velocity gradients, G_b is the generation of turbulence kinetic energy as a result of buoyancy, Y_M represents the contribution of fluctuating dilatation in compressible turbulence to the overall dissipation rate, α_k and α_ε are the inverse effective Prandtl numbers for k and ε and finally S_k and S_ε are user-defined source terms [19].

The discretization of the equations is done by means of Finite Volume Method (FVM). In this method, computational space is divided into smaller elements and surfaces of control volumes are defined on the midplane of each of those elements. By means of Gaussian theory, equations are then integrated over the selected control volume [20].

The type of Finite Volume Method used in the solution of this study is the Cell-Centered Finite Volume Method (CC-FVM). In a CC discretization, solutions are defined at the

center of the primal grid cells (control volumes). Cell center coordinates are defined as the averages of the coordinates of the cell's vertexes. Worthy to note that centroids are not necessarily chosen as cell centers [21].
Figure 2 represents a partitioned control volume for CC-FV discretization.

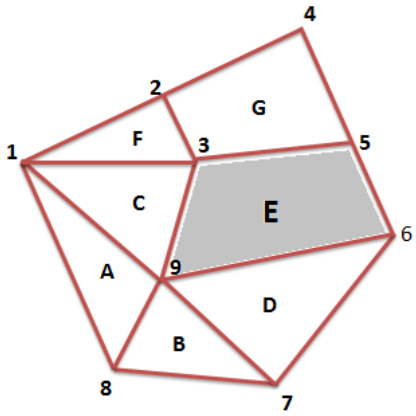

Fig.2. Partitioning of a control volume for finite volume discretization. Numbers 1-9 and letters A-G represent grid nodes and cell centers, respectively. Control volume for Cell-Centered discretization around the cell E is specified with gray color

Using scalable wall function besides a high Reynolds model like RNG k-ε will make y^+ acceptable in range of $30 < y^+ < 300$ [22]. In this range; proper resolution of wall and reduction of running time will be gained simultaneously.

3. Computational Fluid Dynamics (CFD)

3.1. Ordinary H-Darrieus VAWT

Referring to the mentioned turbine in reference [15], a 3D model of that turbine was built with characteristics represented in Table 1.

Completing the geometry construction, a hybrid grid according to Baker's work [23] was applied on the surface of blades for proper wall capture. Also middle parts of the domain were meshed by using unstructured meshing algorithms. Refinements showed that the difference between results is negligible for cell numbers more than 5,545,896. Besides refinements to find proper cell number, some other grid constructions were done with different meshing algorithms to investigate which one is more efficient. Figure 3 illustrates two different grids around leading edge of a single blade. Also Fig. 4 proposes a comparative analysis between different grids.

Table 1. Geometric Characteristics of 3D model

Property	Value
D_{rotor}[m]	3
H_{Blade}[m]	3
Number of Blades (N) [-]	3
Chord Length (C)[m]	0.2
Tip Speed Ratio (TSR)[-]	4
Blade Profile	NACA4415

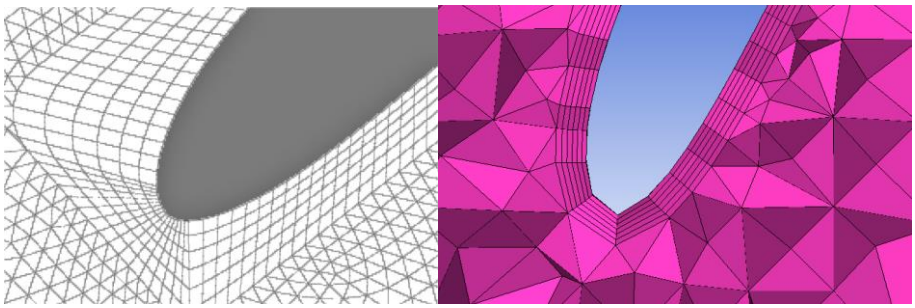

(a) (b)

Fig.3. Different meshing algorithms applied around leading edge of a single blade. (a) Fine hybrid meshing algorithm with trapezoidal elements on the surface. (b) Medium hybrid meshing algorithm with rectangular elements on the surface.

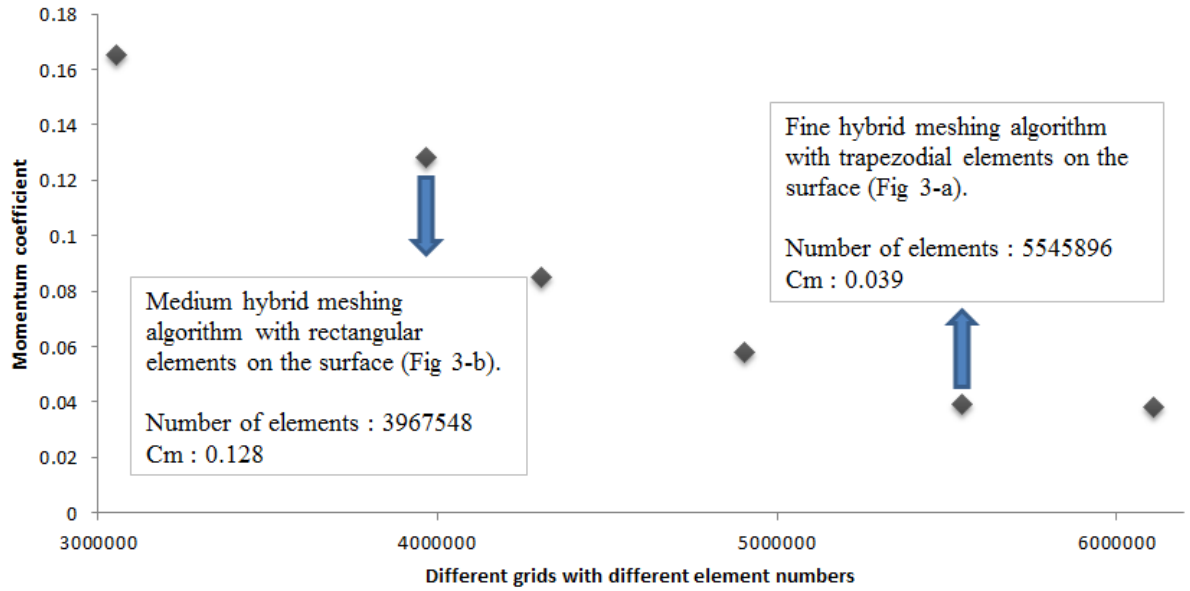

Fig.4. Comparative analysis between different grids

The difference in the results of the last two points is 2.6 % (0.039 and 0.038) which is a negligible number. But the difference in a number of their elements is 562032 elements (5545896 and 6107928) which can result in a significant increase in the running time according to the operative system's abilities. Based on these, the one with 5545896 elements is chosen as the final mesh.

Figure 5 shows the final mesh.

A commercial code has been utilized in order to solve the presented equations.

TSR is formulated as follows:

$$\lambda = \frac{R\omega}{U} \qquad (4)$$

where R is the radius, ω is the rotational speed of the rotor and U is the velocity of free stream. According to Ref. [15] TSR is chosen 4 in this study. Because of constancy of tip speed ratio, radius and inlet velocity, the rotational speed of the rotor will be constant too. In the present work, two different inlet velocities have been chosen for simulation and verification, which are 8 and 10 m/s. In order to gain rotational speed for each of them, equation 4 must be solved for both cases.

According to Courant-Friedrichs-Lewy condition [24], the time step of the solution in both of cases was selected so that the cell convective courant number would be around 1

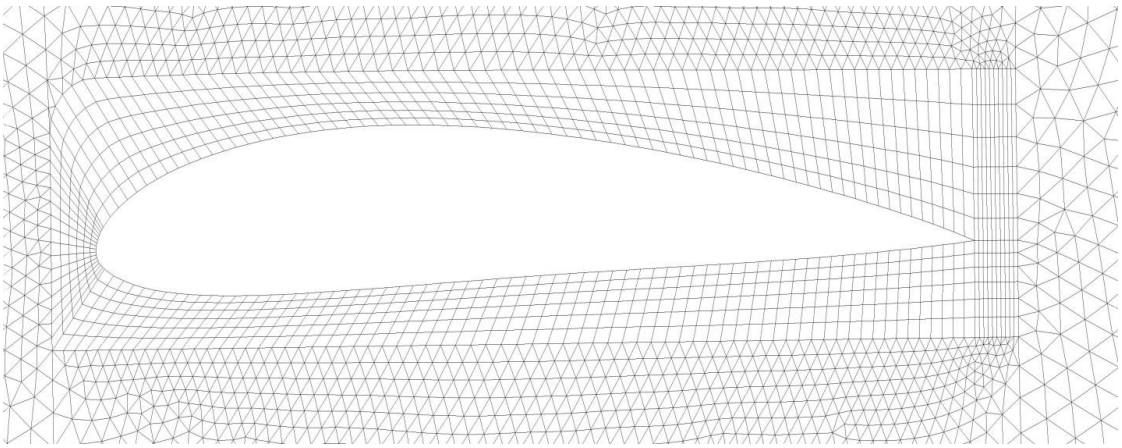

(a)

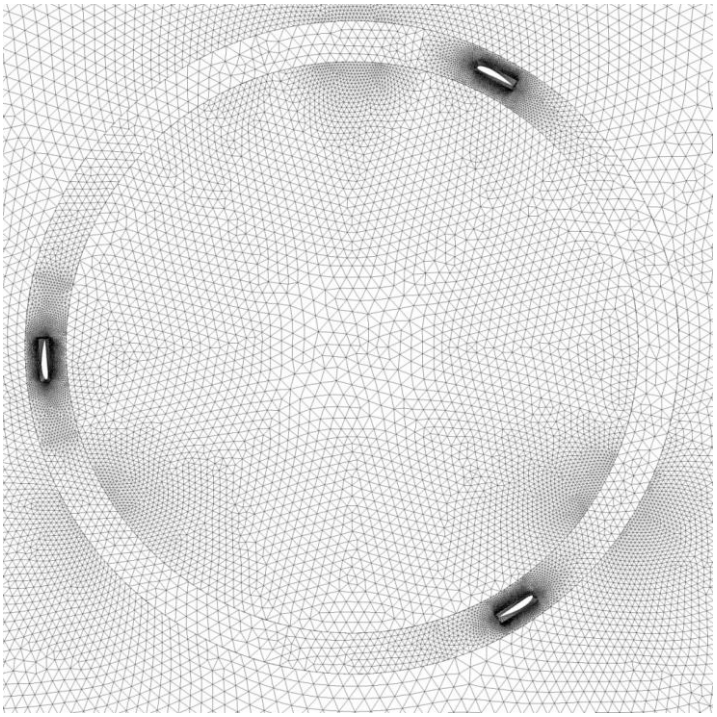

(b)

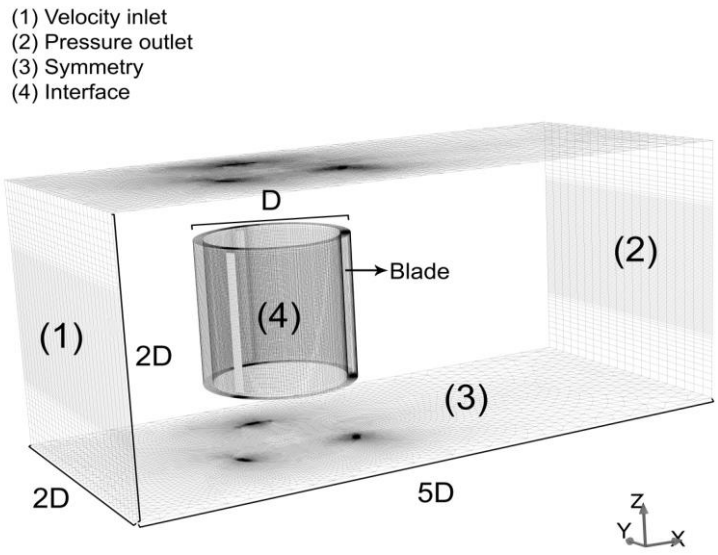

(c)

Fig.5. Generated mesh (a) around blade (b) rotating ring (c) whole 3-D domain with type of boundary conditions and domain size

in the whole domain. This time step was calculated to be 10^{-4} (s) based on the inlet velocity and volume of the tiniest cell in the domain. The rotating algorithm of the rotor was chosen to be Sliding Mesh Model (SMM) based on other studies related to VAWTs [4–7], [17–18] . One considerable point about SMM is that the model does not rely on cell-to-cell match at the interface. For applying this model, a rotating region must be built around all the blades. This region is built by means of two rings, one with a lower radius as the inner ring and one with a bi gger radius as the outer ring. The Boundary condition of both of these rings is the interface. For simulations of this section, radii of the inner ring and the outer ring are 1.4 and 1.6 meters,

respectively. Figure 6 represents the rotating region with inner and outer rings.
All solution methods are shown in Table 2.

The convergence of each time step was directly related to the amount of continuity residual on that time step. This amount was considered to be 10^{-6} for all time steps.

3.2. Doubled-Row H-Darrieus VAWT

As mentioned previously, adding a second row to VAWT is considered as one of the methods of improving the output power of the turbine. This second row is assumed to have the number of blades equal to the first row. In this investigation, the first row is fixed at radius equal to 1.5 meters and second row has two different configurations; first, it has a radius equal to 1.7 meters (0.2 meter distance with the first row) without any angular offset toward first row (completely aligned with the first row) and second, with 60 degrees angular offset. The inlet velocity of both cases is fixed at 8 m/s in this section. Blade characteristics of both rows are exactly the same as those mentioned in Table 1. In this part, coefficients of momentum and power have been chosen as the criteria of comparison between different cases. Since these coefficients can be calculated via a 2D solution, running a 3D solution is not necessary in this part and all calculations are done two-dimensionally.

Fig.6. Rotating region

Table 2. Solution Methods

Property	Value
Pressure-Velocity Coupling	SIMPLE
Spatial Discretization	
Gradient	Least Squares Cell-Based
Pressure	Second Order
Momentum	Second-Order Upwind
Turbulent Kinetic Energy	First Order Upwind
Turbulent Dissipation Rate	First Order Upwind
Transient Formulation	First Order Implicit

3D schematic view of the aligned doubled-row H-Darrieus VAWT is shown in Fig.7.

The dimension of the simulation domain in this section is exactly as the previous section without third dimension (Fig. 5.c). Also, the generated mesh is exactly the same with 2-D cross section of previous mesh (Figs. 5.a and 5.b) except the addition of the second row of blades which is the only difference. After refinements, the grid showed negligible changes in results for cell numbers in range 57759 - 486912 cells. Table 3 represents changes versus grid size. All the following cases in Table 3 are simulated with an inlet velocity of 8 m/s.

All simulations are done by applying RNG k-ε turbulence model as the previous section.

Characteristics of pressure-velocity coupling and spatial discretization are exactly the same as those mentioned in Table 2.

According to the presented results in Table 3, the grid size equal to 57759 was selected; two final simulations are done in this part, first for the aligned case and second for the case with 60 degrees angular offset.

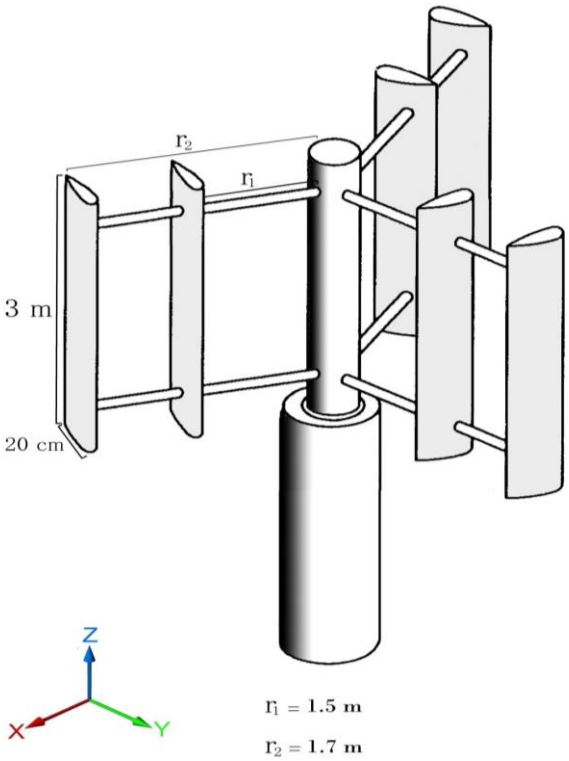

Fig.7. 3D schematic view of the aligned doubled-row H-Darrieus VAWT

Table 3. Grid Study

Cell Number	Coefficient of Momentum
21109	0.220
30704	0.209
45862	0.165
52139	0.144
57759	0.132
190687	0.131
486912	0.131

4. Results and Discussion

4.1. Ordinary H-Darrieus VAWT

After analyzing the results, "Torque-Time" plot will be exploited. According to the mathematic relation between torque and power, multiplying the plot by the rotational speed will result in the "Power-Time" plot. Finally, the average of this gained plot is the average cyclic power of the turbine.

Mathematic equation of the coefficient of momentum for an ordinary H-Darrieus VAWT is as follows:

$$C_m = \frac{T}{\frac{1}{2}\rho A R U^2} \tag{5}$$

where T is torque, ρ is the air density, R is rthe adius of rthe otor, A is swept area of the rotor zone and U is vthe elocity of fthe ree stream. The selection of this coefficient as a comparative tool is based on other studies using the same coefficient for comparison of different cases [7], [12], [14].

Besides the momentum coefficient, the power coefficient is also calculated to present the capability of each case more sensibly. Mathematic formulation of this coefficient is as follows (for an ordinary H-Darrieus VAWT):

$$C_P = \frac{P}{\frac{1}{2}\rho A U^3} \tag{6}$$

According to outputs of reference [15], comparison between the average power of present work and that of reference [15] could be done. Table 4 represents the outputs of the present work.

Also Fig. 8 represents the "Power – Inlet velocity" curve gained via BEM theory in Ref. [15] and also a comparison between different results.

Table 4. POWER OUTPUTS OF PRESENT WORK (NUMERICAL APPROACH)

Free Stream velocity (m/s)	Rotational Speed (rad/s)	Average Cyclic Torque (N.m)	Coefficient of Momentum	Coefficient of Power	Average Cyclic Power
8	21.33	22.7	0.042	0.168	484.21 W
10	26.66	32.96	0.039	0.156	878.98 W

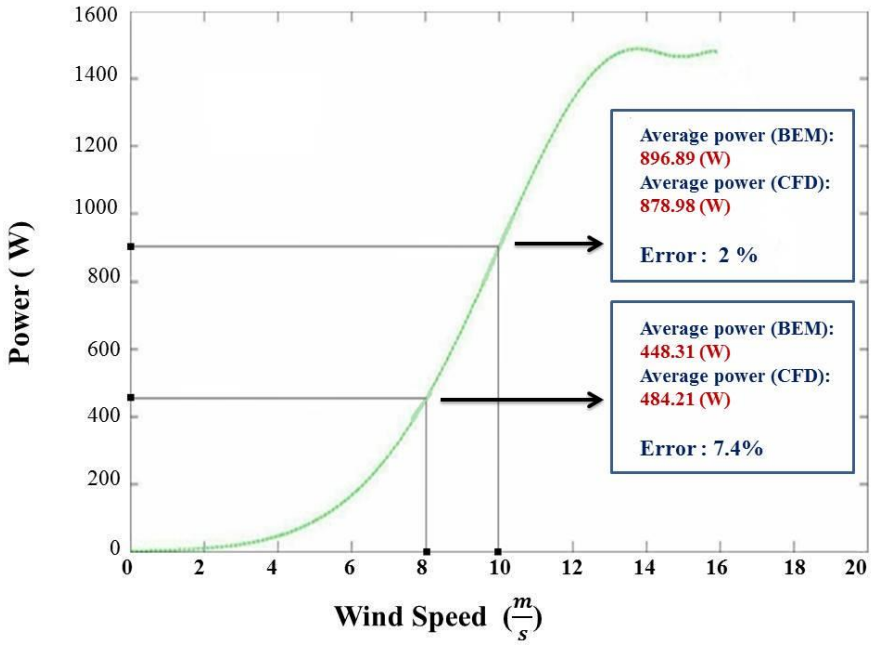

Fig.8. "Power-Wind Speed" plot of [15] extracted via BEM

Power equation obtained according to BEM theory is as follows [15]:

$$Power(W) = 302.2\exp\left(-\left(\frac{V-16.5}{1.242}\right)^2\right) + 1484\exp\left(-\left(\frac{V-13.69}{5.2}\right)^2\right) \quad (7)$$

By substituting V=8 m/s and V= 10 m/s as inlet velocity in equation above, output power will be gained respectively 448.31 and 896.89 W. According to Table 4; average output power obtained by CFD for inlet velocities of 8 and 10 m/s respectively is: 484.21 and 878.98 W. As it is depicted in Fig. 8, mean error between analytical approach (BEM) and CFD is different in two simulated cases (7.4% for inlet velocity of 8 m/s and 2% for inlet velocity of 10 m/s). Results demonstrate that RNG k-ε turbulence model proposes more similarity to analytical results in higher velocities but definitely, more researches should be done experimentally, numerically and analytically to testify this.

According to the operative system's information which was mentioned in section 3.1, the running time of each of these 3D simulations was around 1200 hours. Based on the acceptable accuracy of the comparisons above and also a considerable amount of running time, no urgency was felt to run the third simulation in order to compare another inlet velocity.

Contours of static pressure, velocity magnitude and turbulence intensity for a single time step are represented in Fig. 9. It must be noted that the rotation is considered counterclockwise.

As it is obvious in the above figure, at the leading edge of the nearest blade to the entrance of the flow, the most amount of pressure increase is detected (Fig. 9.a). After this incident, what happens in the downstream of the first blade is mostly visible in Fig. 9.b; where the starting of the wake region is observable. Also in Fig. 9.c it can be found that in two other blades, the one which moves in the direction of the free stream has more influence on increasing the turbulence intensity than the other one which moves in the opposite direction.

Also, wall y^+ histogram is depicted in Fig. 10.

4.2. Doubled-Row H-Darrieus VAWT

For a doubled-row VAWT, swept area of the rotor will change into:

$$A = D_{Outer}\, H = 2R_{Outer}\, H \quad (8)$$

where H is the height of the rotor (blade).

The effective radius of a doubled-row H-Darrieus VAWT is the radius of outer row (because this radius creates swept area), so R in the Eq.(5) will also be substituted with R_{Outer}. Finally, the formulation of C_m for a doubled-row VAWT will change into this:

$$C_m = \frac{T}{\rho R_{Outer}^2 HU^2} \quad (9)$$

It is necessary to mention that for a 2-D simulation, H is considered 1m. Also based on equations 5 and 6, the coefficient of power can be formulated as follows:

$$C_P = C_m * TSR \quad (10)$$

So in order to calculate the value of C_p for a doubled-row case, the value of C_m must be multiplied by TSR (4 in this study). A comparison of these criteria between cases will clarify which case has better performance than other cases. The"Momentum Coefficient-Revolution Time" curve for both of doubled-row cases (for inlet velocity of 8 m/s) is represented in Fig. 11.

As it can be seen in Fig. 11, each cycle has 3 peaks that each peak fills a 120-degree period. Little difference between the peak values is due to high sensitivity in ups and downs which requires a much smaller time step (which is not necessary) to capture jumping from first 120-degree period to the second one. Since the percentage of difference is less than 5%, this difference could be assumed negligible.

Table 5 represents average C_m and C_P for both of cases.

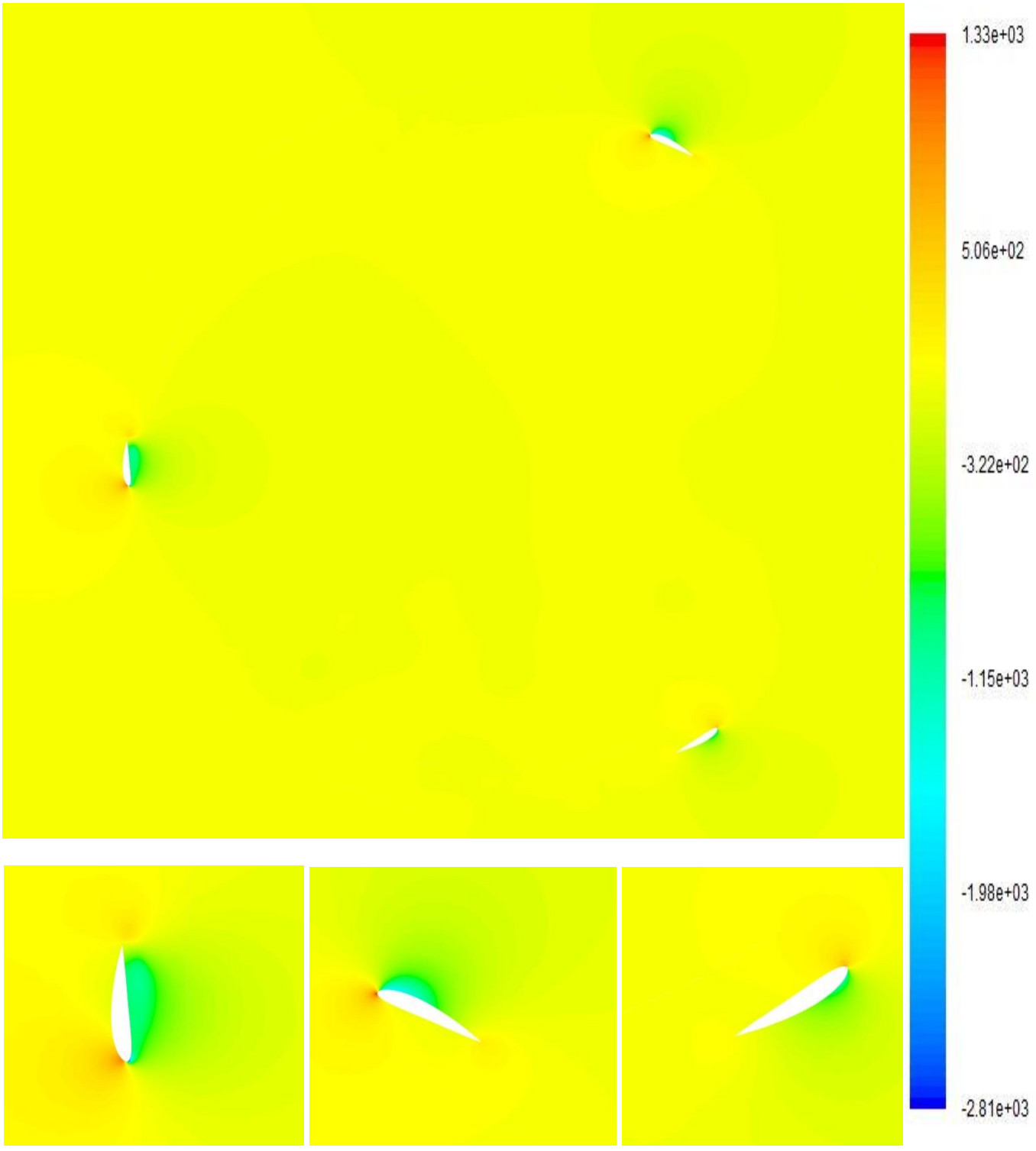

(a)

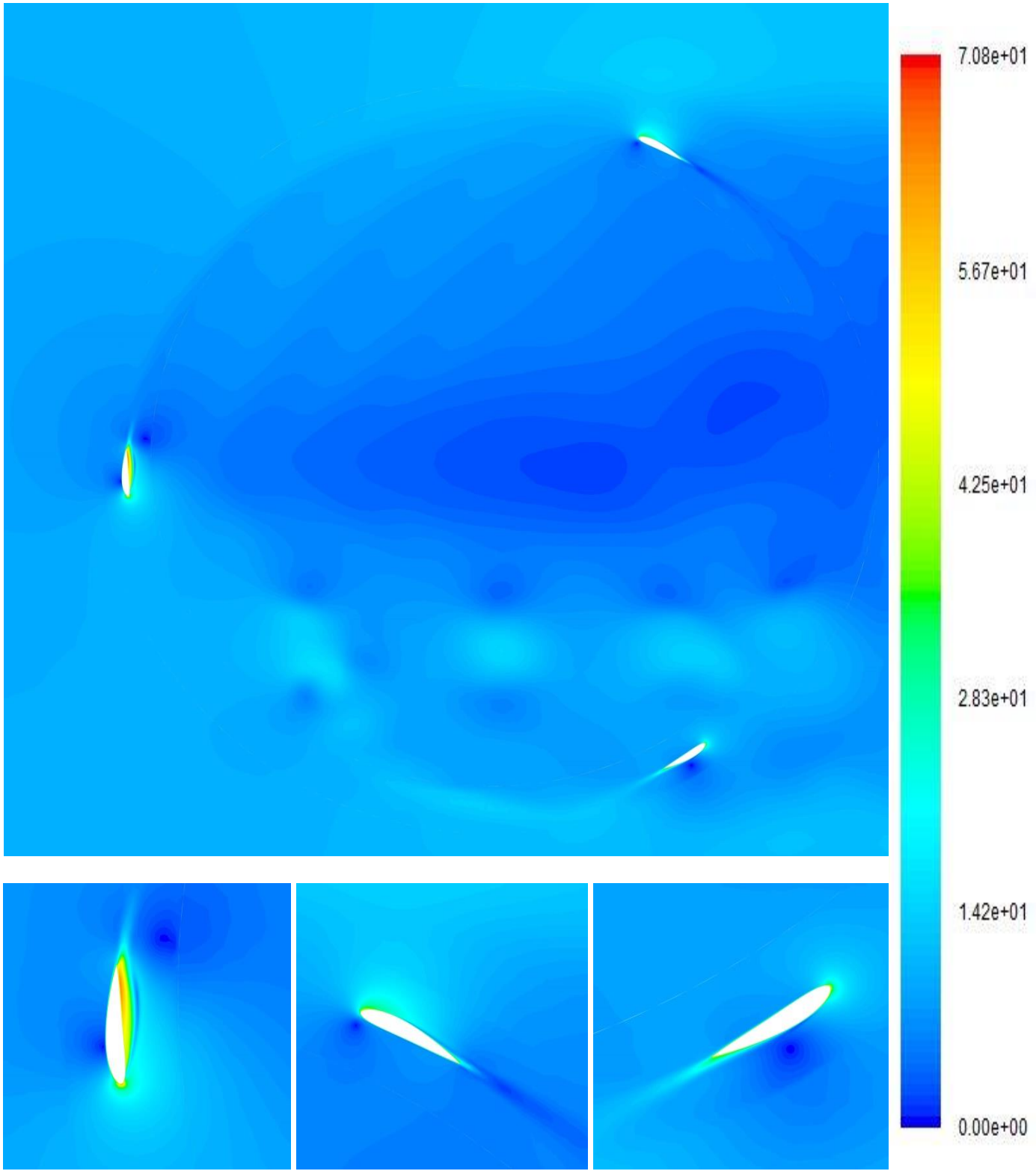

(b)

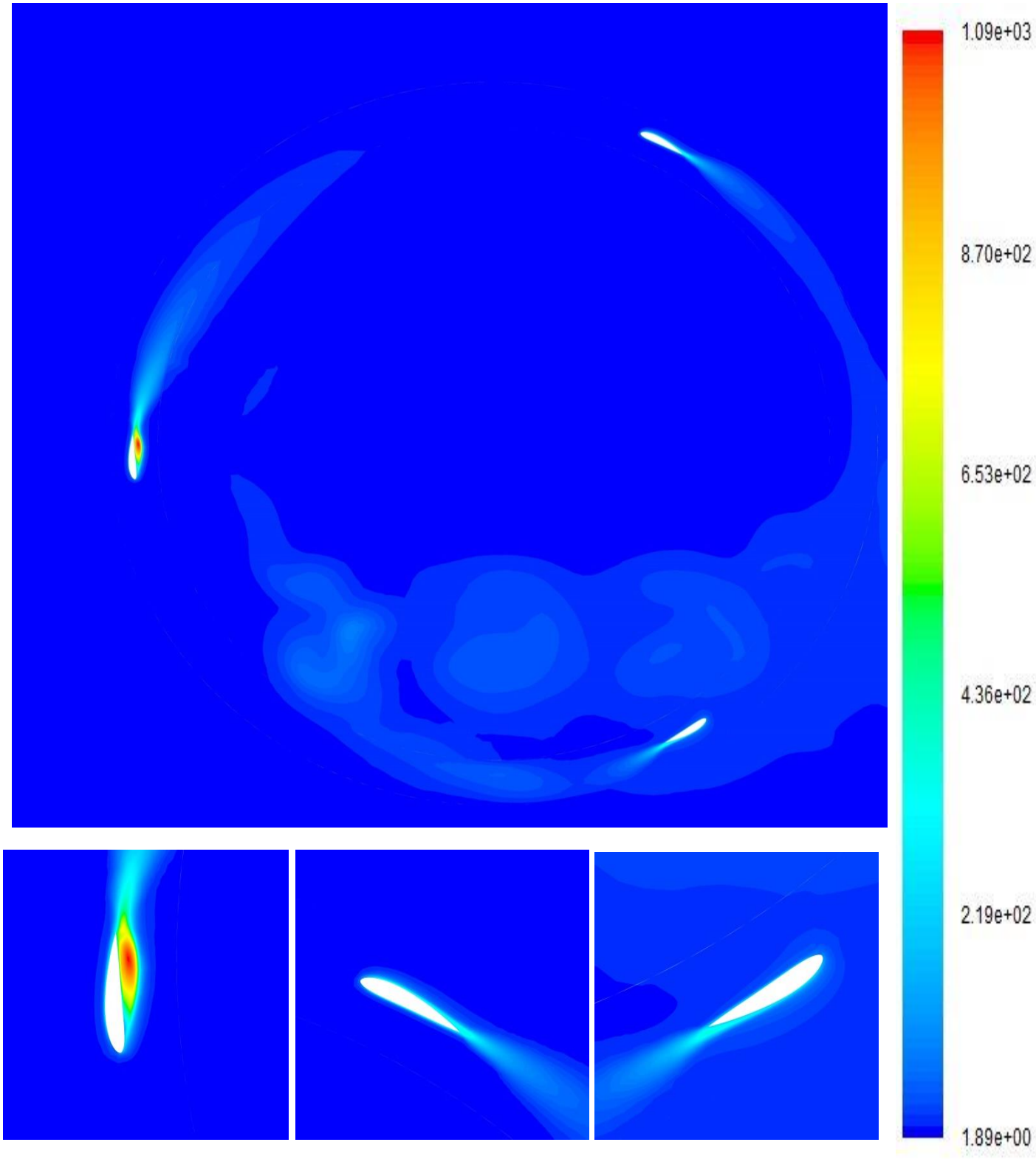

(c)

Fig.9. Contours of (a) Static pressure (Pa) (b) Velocity magnitude (m/s) (c) Turbulence intensity (%)

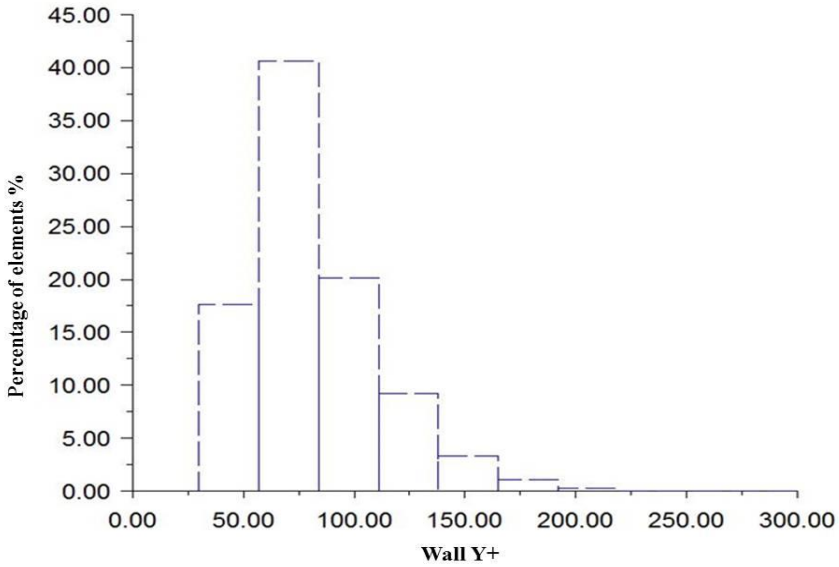

Fig.10. Wall Y+ histogram

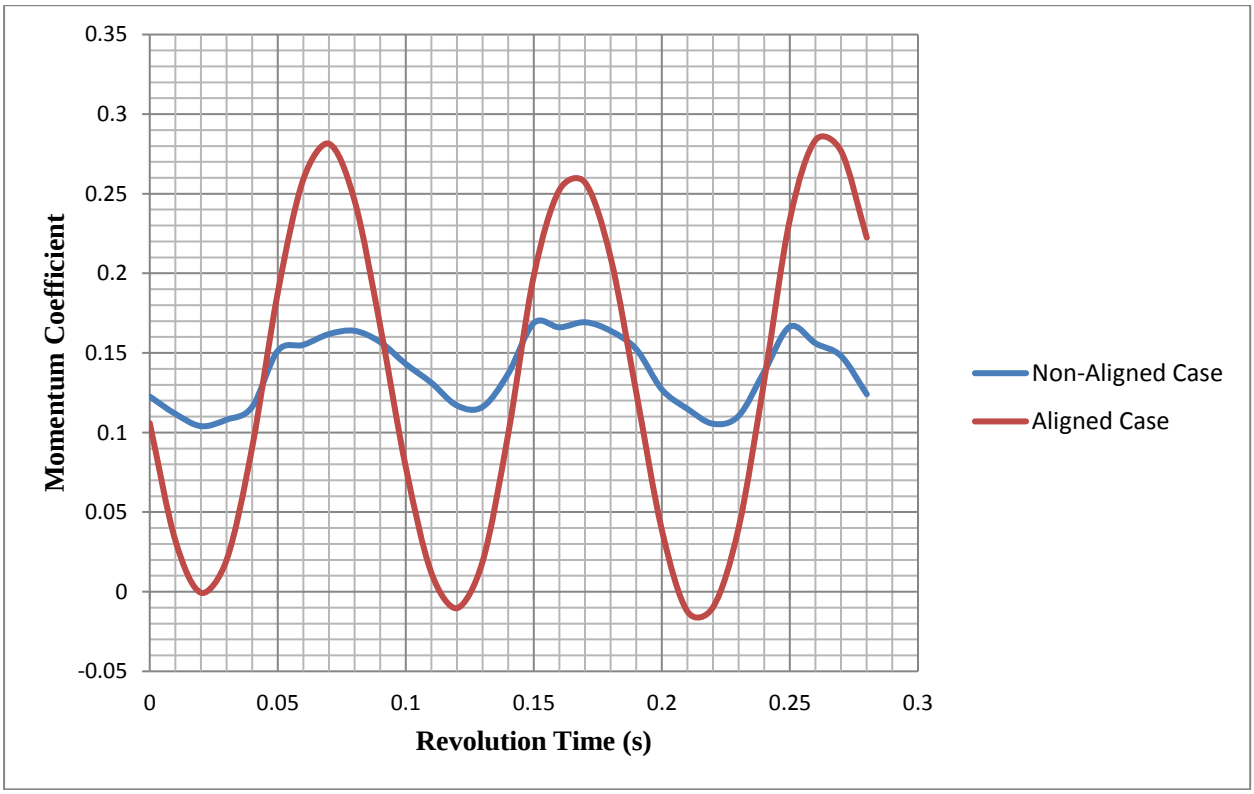

Fig.11. "C_m – Revolution Time" plot for aligned and non-aligned doubled-row H-Darrieus VAWTs for inlet velocity of 8 m/s.

Table 5. Average C_m of Simulated Cases

Case	Average C_P	Average C_m
R_2 =1.7 , R_1 =1.5, Offset=0°	0.528	0.132
R_2 =1.7, R_1 =1.5, Offset=60°	0.532	0.133

Contours of static pressure, velocity magnitude and turbulence intensity for both aligned and non-aligned cases are depicted in Figs. 12 and 13.

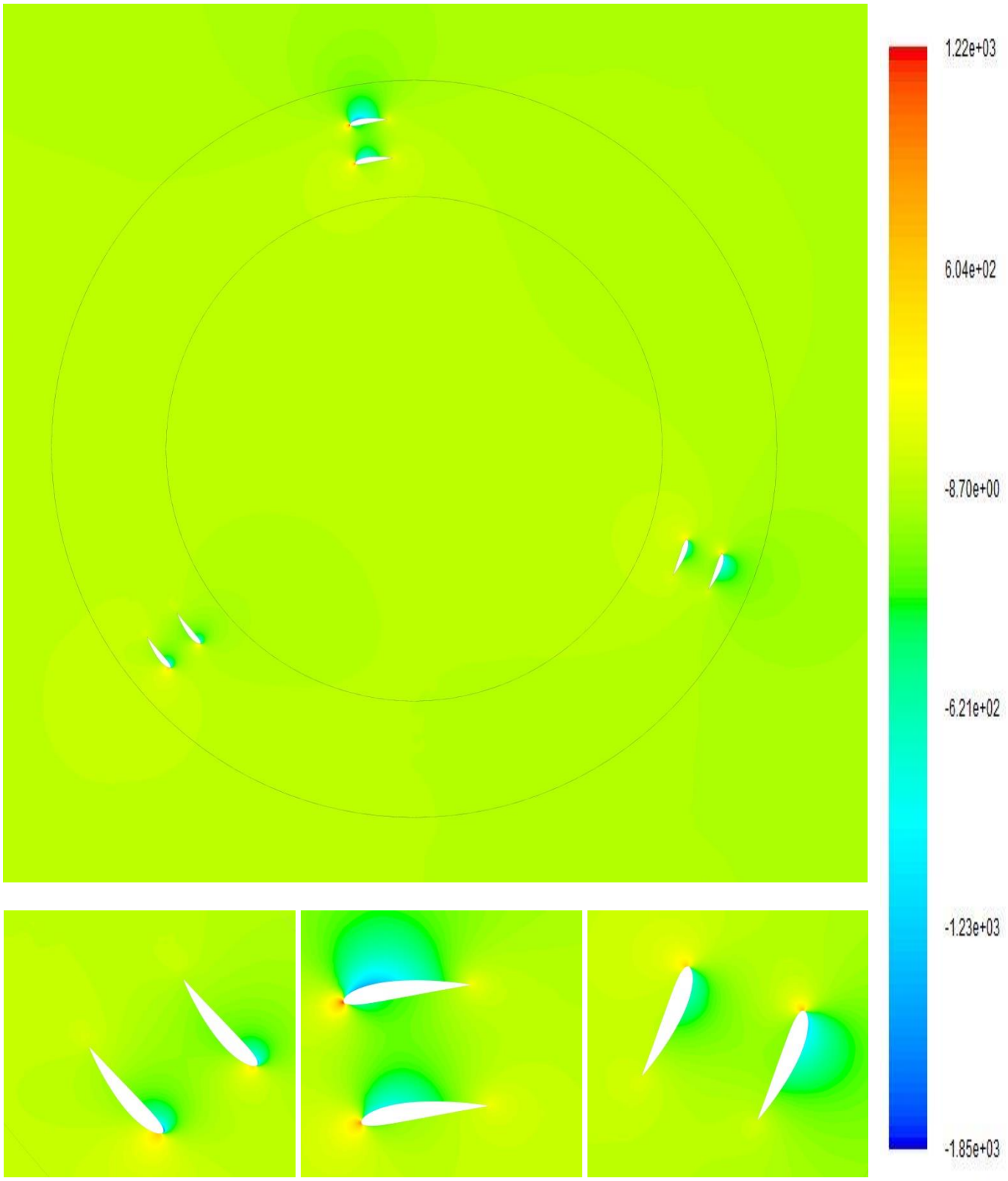

(a)

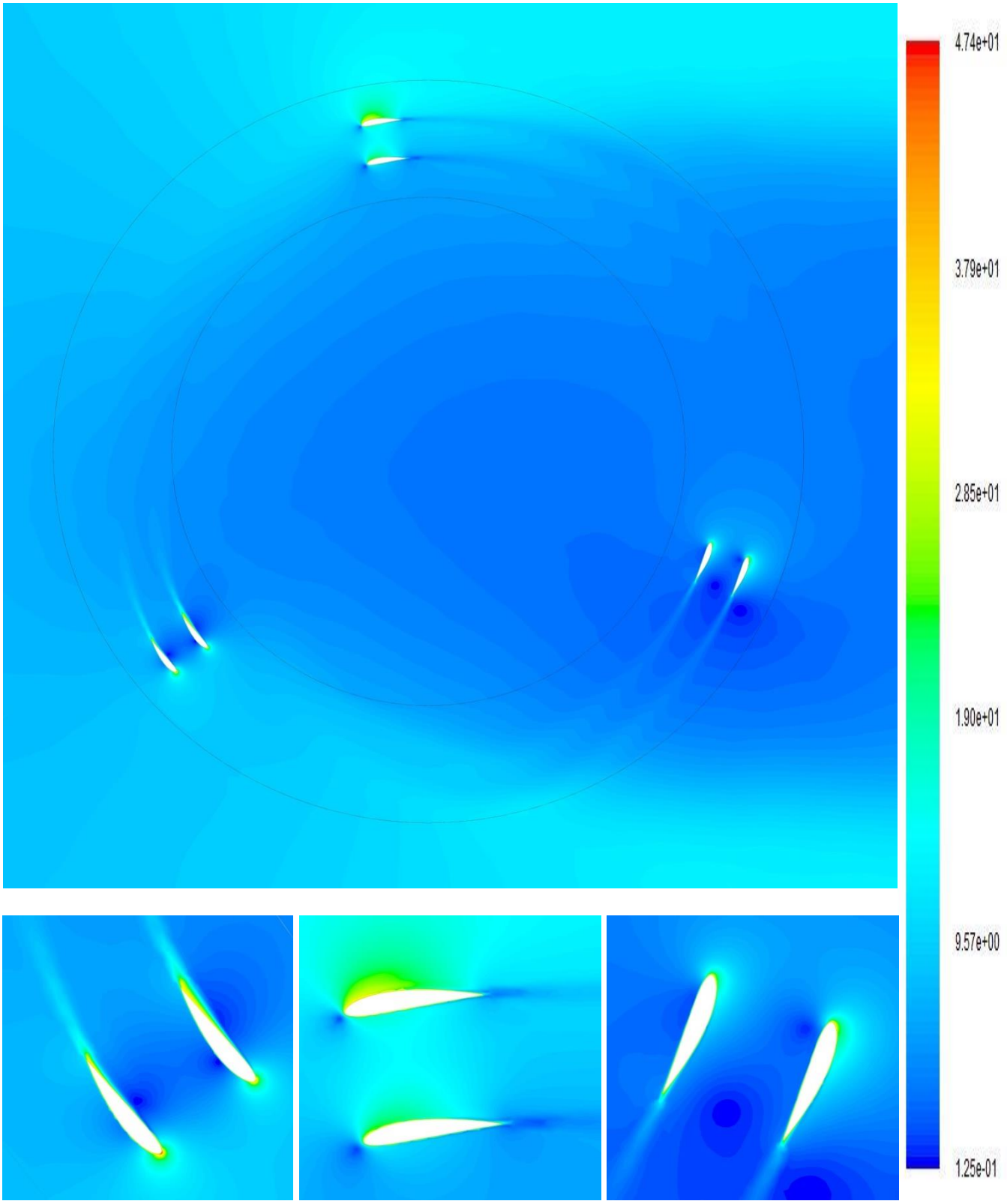

(b)

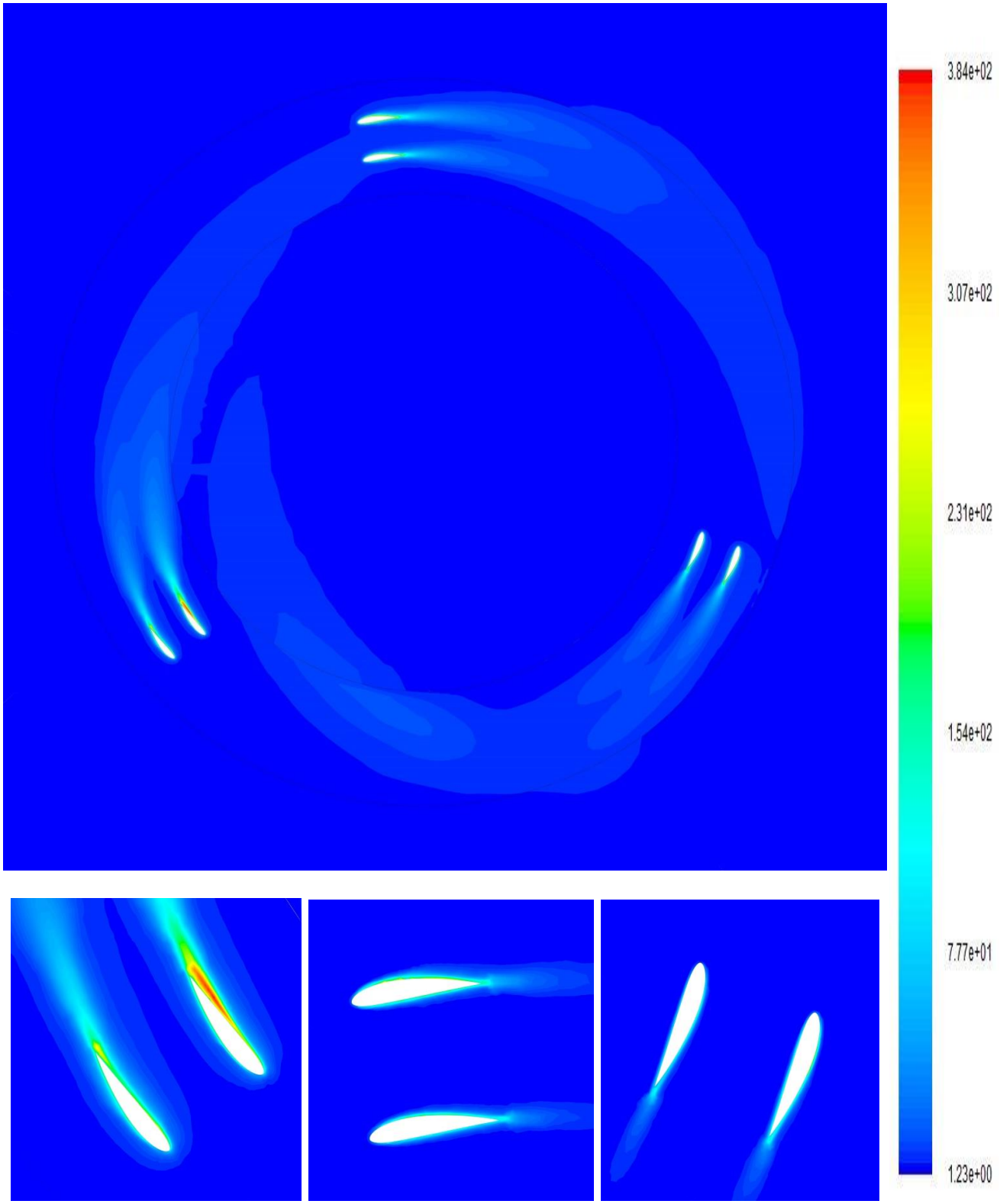

(c)

Fig.12. Contours of aligned case. (a) Static pressure (Pa) (b) Velocity magnitude (m/s)
(c) Turbulence intensity (%)

The closest leading-edge moving toward the entrance of the flow is the place where the most increase in pressure contour is visible (Fig. 12.a). Also around the leading edge of the other blade which is under the mentioned one (located in the first row), another increase in pressure (less than the previous one) is detected. After the incident of the flow with the first couple of blades, the starting of the wake region is obvious in Fig. 12.b. Thickness of this wake region is approximately equal to the distance between an upper couple of blades and downer couple which is rational because out of this distance, there is no obstacle in the flow channel to cause a wake. Fig. 12.c also shows that the downer couple of blades has more effect on increasing the turbulence intensity.

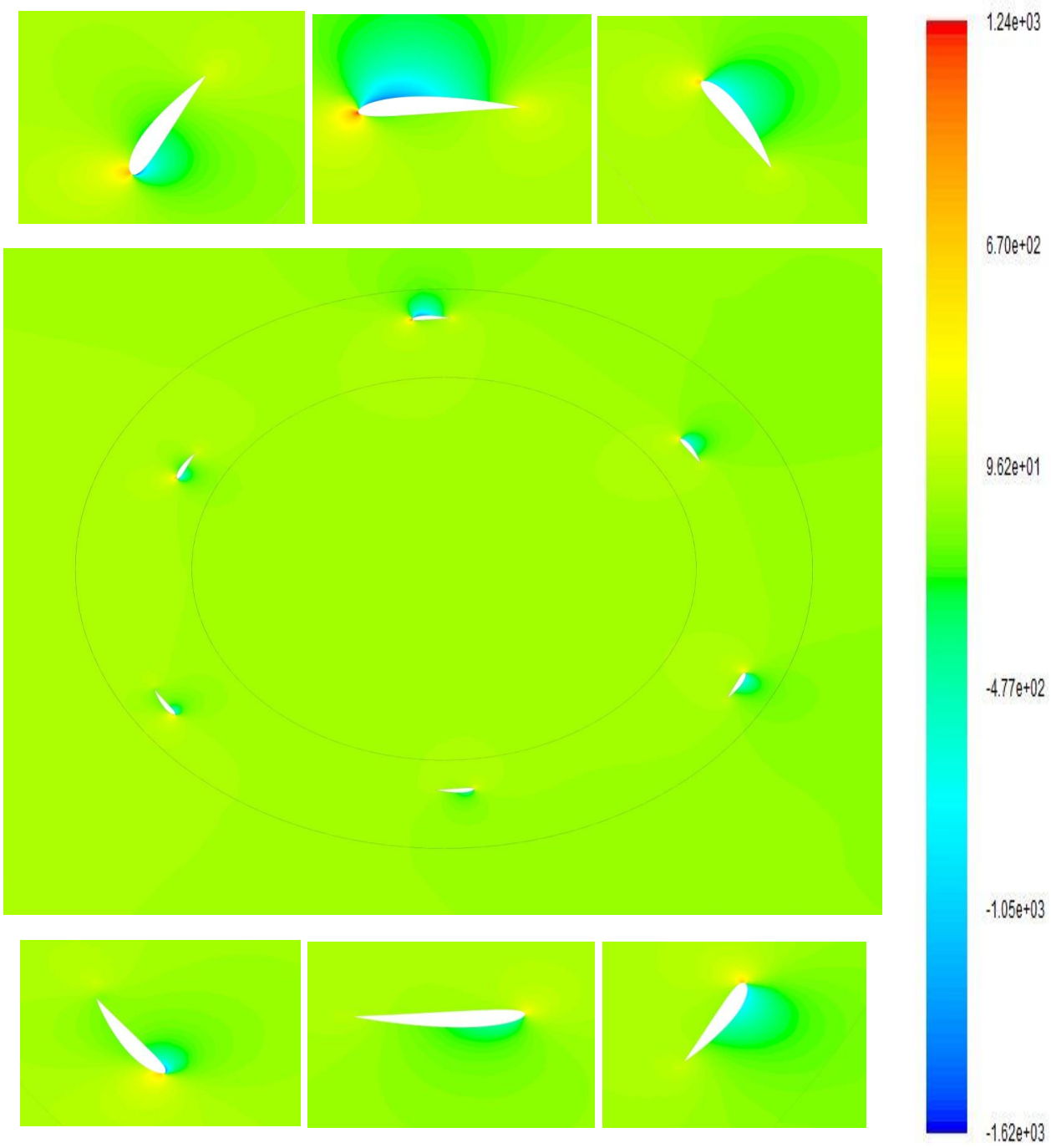

(a)

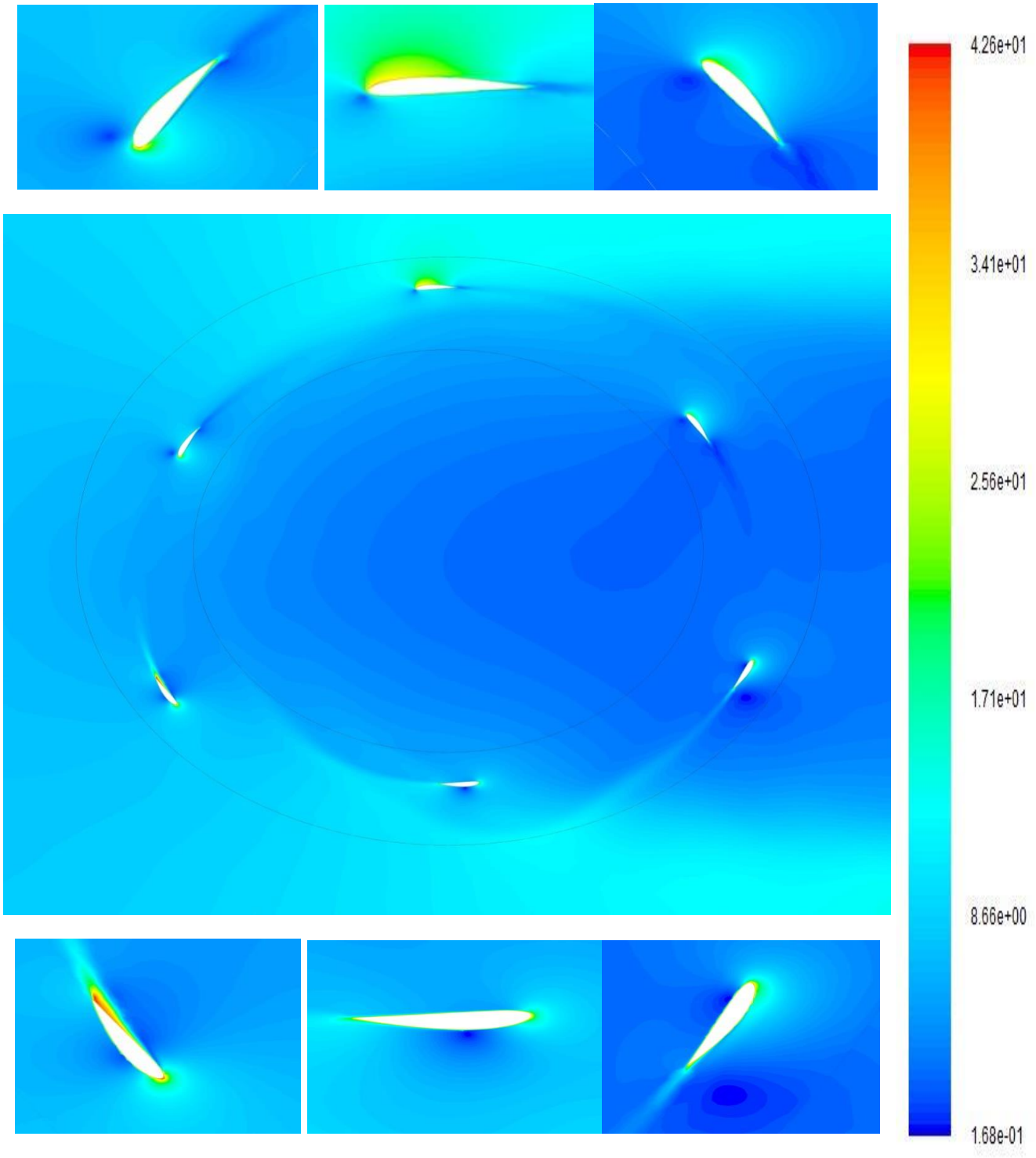

(b)

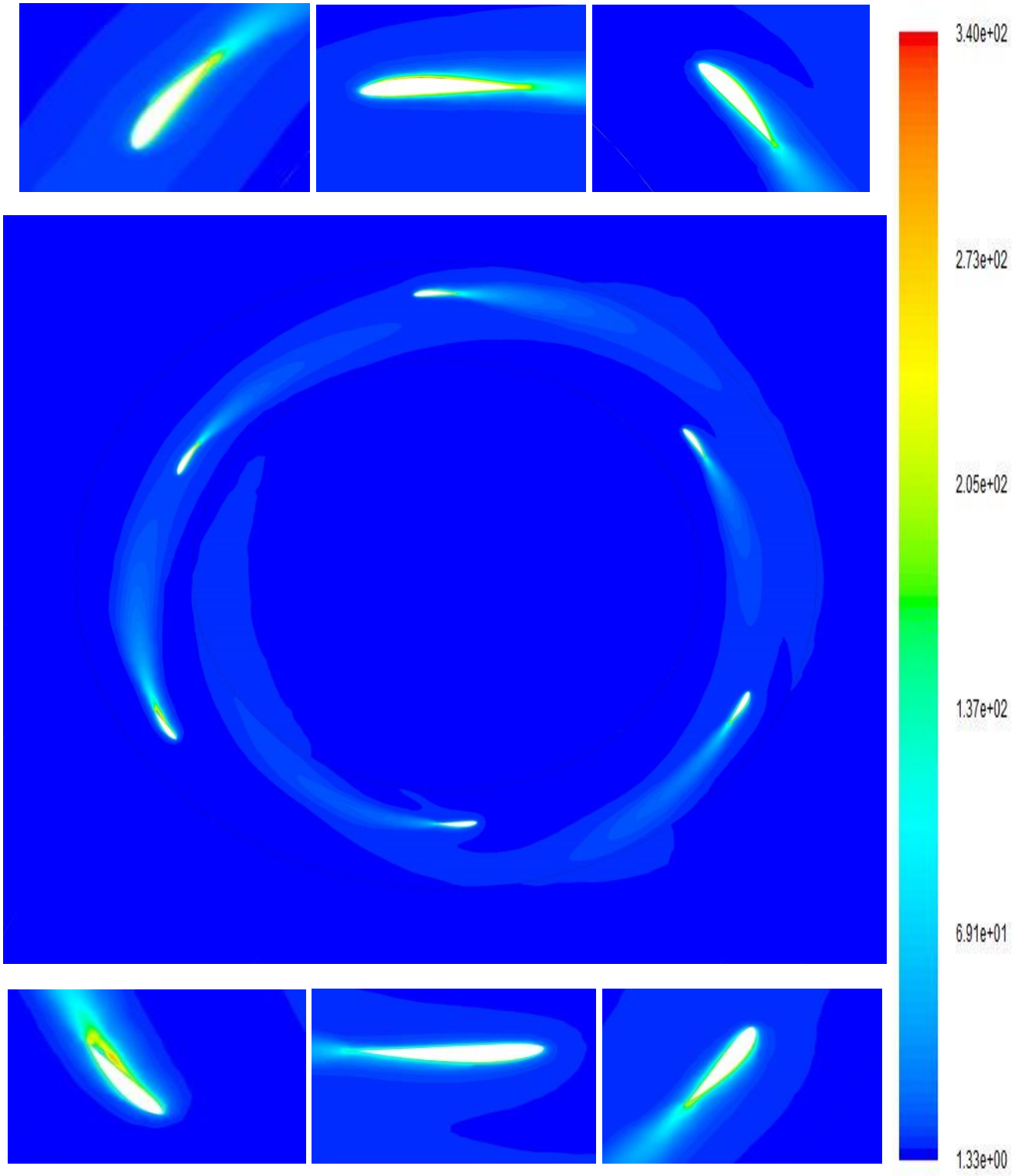

(c)

Fig.13. Contours of non-aligned case. (a) Static pressure (Pa) (b) Velocity magnitude (m/s) (c) Turbulence intensity (%)

In Fig. 13.a, it can be observed that between leading edges facing the flow prior to others, the one with less angle of attack toward the direction of the free stream experiences more pressure increase than other leading edges with more angle of attack. In Fig. 13.b, the thickness of the wake region is the same with the distance between the upper blade and the downer one. Fig. 13.c also shows that in a non-aligned case, every single blade has less effect on amplifying the turbulence intensity than the effect of a couple of blades in aligned cases (Fig. 12.c).

Comparison of averaged C_m and C_p of doubled-row and ordinary H-Rotor, Darrieus VAWT will make the difference of these two more clear. For introduced turbine in Ref. [15], "$C_m - Revolution\ Time$" plot that is obtained by CFD analysis, is represented in Fig. 14 for inlet velocity of 8 m/s. It must be mentioned that all comparisons of this section are based on an inlet velocity of 8 m/s because this velocity was used for doubled-row VAWT simulations.

Average value of C_m in the above plot is 0.042 ($C_p = 0.168$), whereas according to Table 5, the average value of C_m for doubled-row VAWTs simulated in this work is about 0.132 ($C_p = 0.528$). This means that the addition of a second row with a radius of 1.7 meters either with or without angular offset will improve the performance of the H-Rotor Darrieus VAWT about 314%. According to reference [14]; addition of an auxiliary airfoil (with smaller chord length) to an ordinary three-bladed Darrieus VAWT (for free stream velocity of 11 m/s) caused the maximum momentum coefficient to jump from 0.043 to 0.145 (337% increase) . Comparing these two percentages is an approximate verification of the accuracy of this study.

According to the results represented, the coefficient of momentum has been significantly improved after adding the second row. But it has to be considered that in a doubled-row VAWT, more use of horizontal solid bars, blades, and joints is needed and thus more mass is expected. Among two types of doubled-row VAWTs, aligned type requires less horizontal solid bars in comparison with non-aligned type since in aligned type a single bar goes through both rows from central shaft (as it is depicted in Fig. 7).

On the other hand, when a single bar is loaded by two blades, because of more mass-loaded, more bending is expected on bars in aligned type.

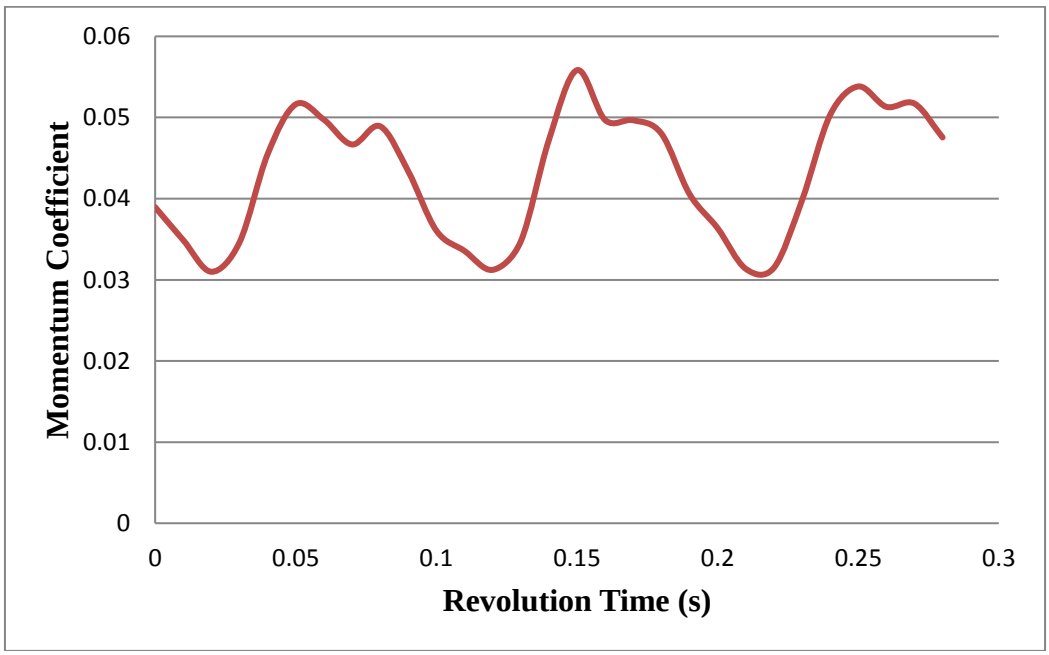

Fig.14. "C_m − Revolution Time" plot of VAWT introduced in Ref. [15] extracted via CFD simulation for inlet velocity of 8 m/s

Proper maintenance of connecting bars and joints is very important in doubled-row VAWTs. Also, appropriate selection of solid materials must be considered. The advantage of more extracted power can turn into a disadvantage if continuous preservation is not applied.

5. Supporting Studies

In order to evaluate the accuracy and efficiency of this study, several more simulations (with some modifications in comparison with the main cases) are done to compare the achieved results with results out of modified simulations. In these new simulations, the following parameters are modified:

1- Turbulence model: SST k-ω and Spalart-Allmaras turbulence models are also taken into account.
2- Domain dimensions: Length of the domain has been changed from 5D to 10D and 20D. Also other dimensions are increased with the same ratios.
3- Solution methods: Changing first-order scheme to second order.
4- Geometry: Central shaft of the rotor zone has been added to the geometry and final mesh in order to analyze its influence on the values of the mentioned criteria.

Table 6 represents the results of all these new simulations with their running time. Besides all solution conditions, considering the running time in this table can be an appropriate criterion to apply a trade-off between the required time and required accuracy. All these simulations are done two-dimensionally for aligned geometry.

Running times of the above table are calculated from the starting point till the convergence point, where the turbine behaves almost similar (less than 5% error) in the last 3 cycles. Also, it has to be mentioned that the Spalart-Allmaras model resulted in negative torque in most of the calculative time steps. Since this model did not face convergence in this study, no data can be proposed as a result of this model.

Analyzing the effect of the central shaft on the output values, it can be seen that the results express a good similarity to results out of recent research [25]. Also by assuming the regular shaft diameter less than 20 cm for a Darrieus VAWT with mentioned dimensions, it can be seen that the maximum relative error between the main case (geometry without central shaft) and the case with the central shaft is less 10% which is an acceptable maximum relative error.

Figure 15 represents the relationship between the power coefficient and the central shaft's diameter.

Table 6. Comparative study between different cases

Case Characteristics	Relative Error %	C_m	C_p	Running Time
RNG k-ε (utilized in this study)	0	0.132	0.528	74 hours
SST k-ω	18	0.108	0.432	92 hours
Spalart-Allmaras	———	—	—	42 hours
RNG k-ε (using second order scheme)	2	0.135	0.54	83 hours
SST k-ω (using second order scheme)	9	0.12	0.48	109 hours
10 D domain length (RNG k-ε - First order)	9	0.121	0.484	104 hours
20 D domain length (RNG k-ε - First order)	11	0.117	0.468	201 hours
Considering central shaft with D=0.2 m length (RNG k-ε - First order)	10	0.118	0.472	78 hours
Considering central shaft with D=0.3 m length (RNG k-ε - First order)	15	0.114	0.456	78 hours
Considering central shaft with D=0.5 m length (RNG k-ε - First order)	28	0.095	0.38	76 hours

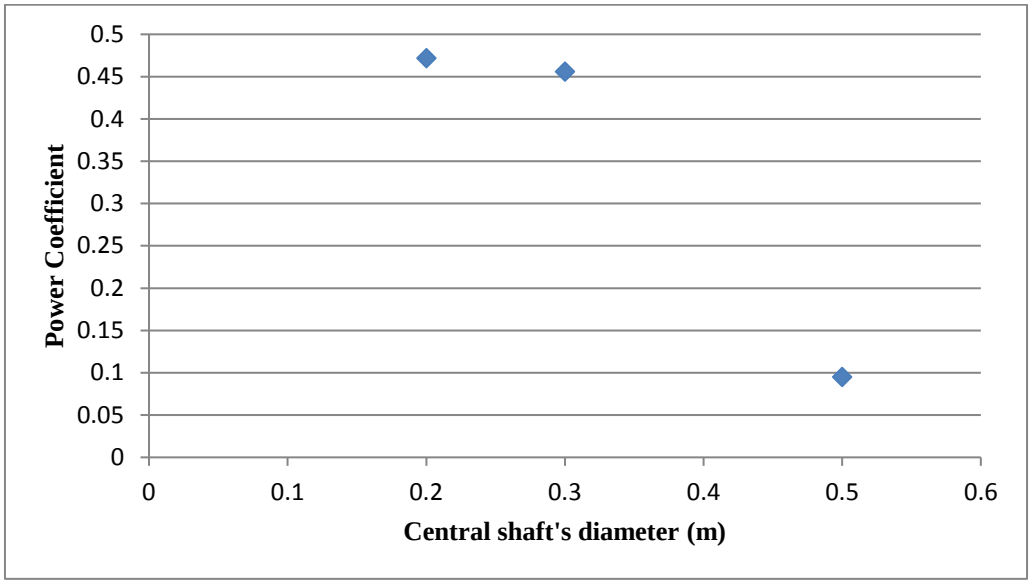

Fig.15. "Power coefficient-Central shaft's diameter"

Also Fig. 16 depicts the velocity contour for the case having results with the biggest deviation toward the main case's results ($D_{Shaft} = 0.5\ m$, Relative Error: 28%). It is obvious that formation of such wake region can justify this 28% deviation. In order to highlight the effect of central shaft, this contour is represented with banded coloring.

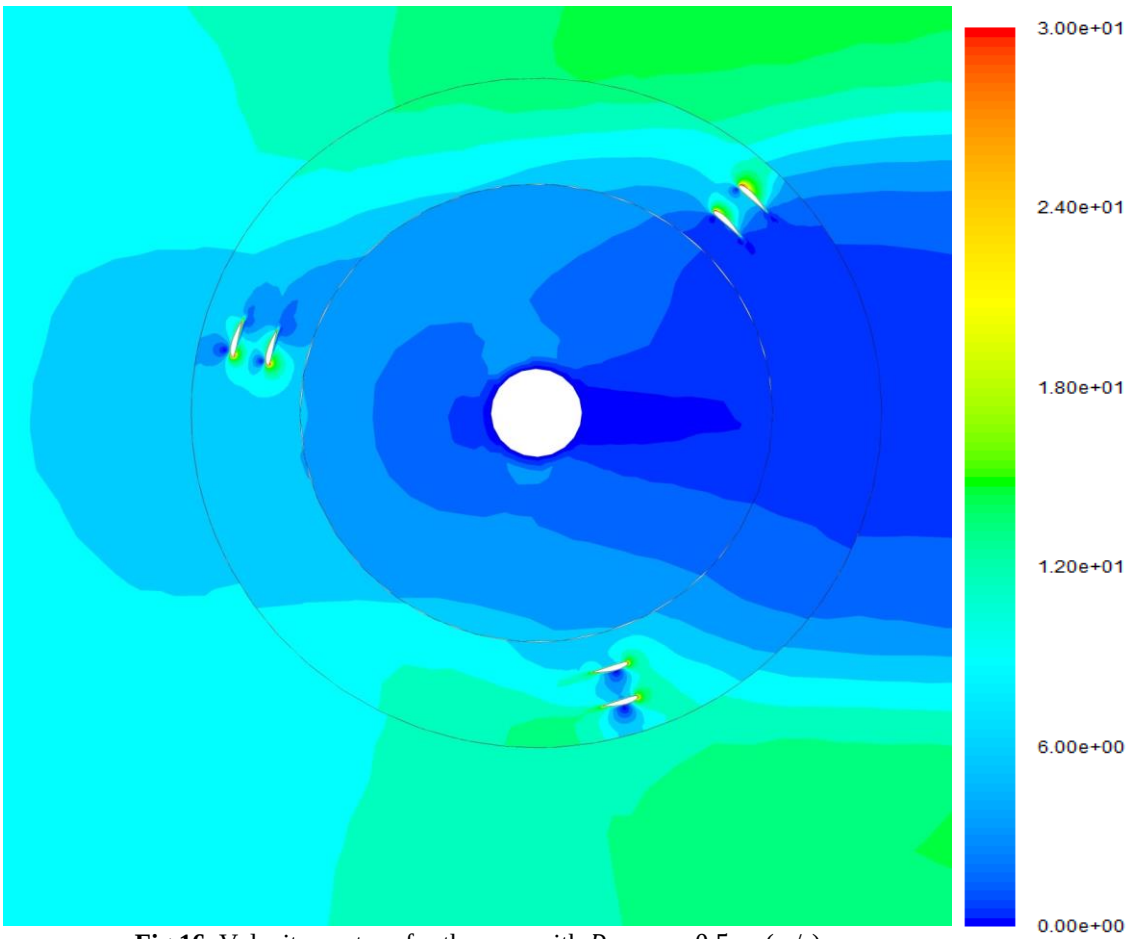

Fig.16. Velocity contour for the case with $D_{Shaft} = 0.5\ m$ (m/s)

Also by investigating the results of the cases with modified domain size (L=10D and L=20D), it can be seen that the percentage of running time's increase is more than the percentage of momentum coefficient's decrease and a trade-off will justify the usage of the main domain (L=5D).

Figure 17 depicts the velocity contour for cases with modified domain size.

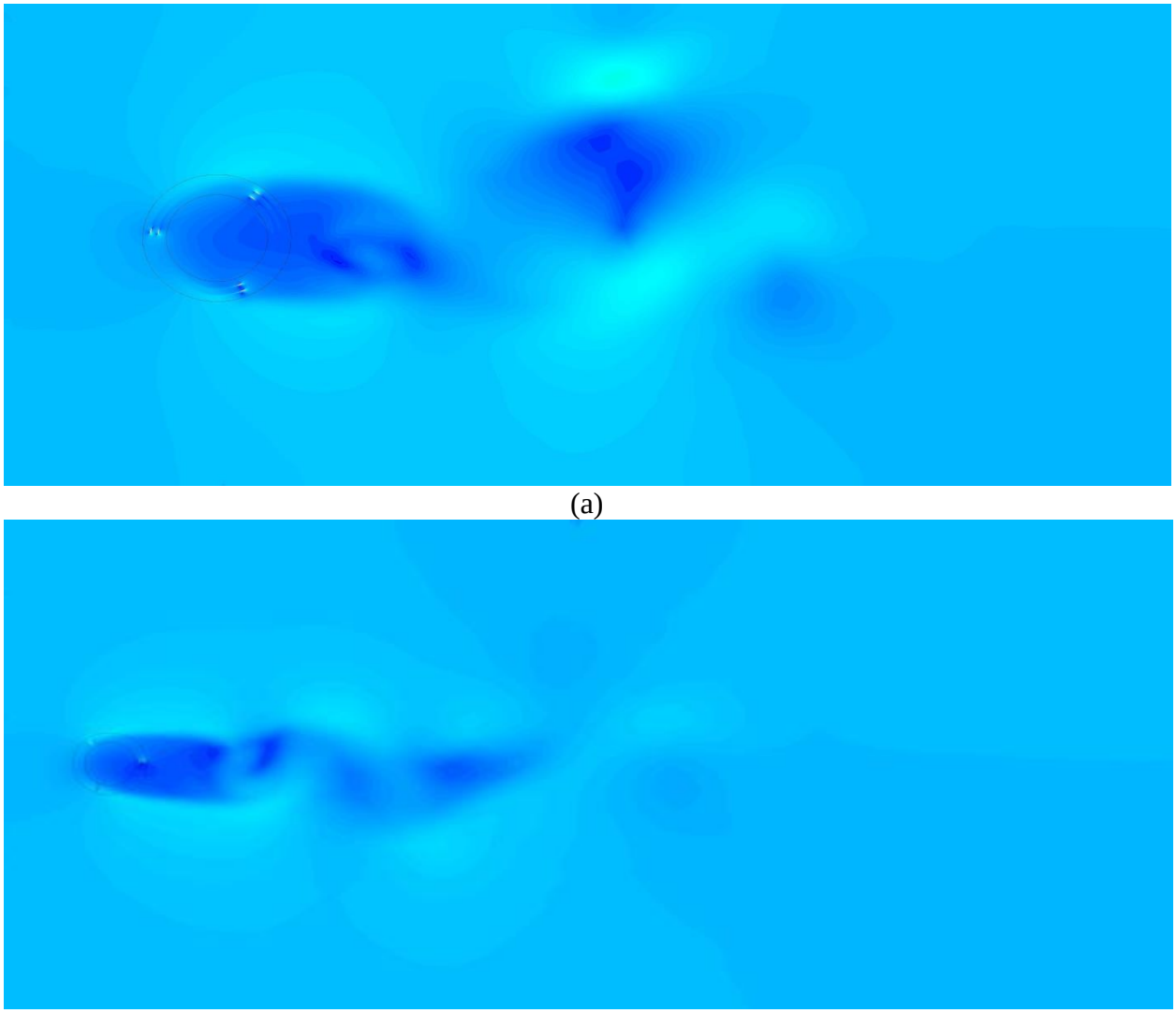

(a)

(b)

Fig.17. Velocity contour of cases with modified domain size (a) L=10D (b) L=20D

Considering all mentioned studies, it should be noted that another strong basis on which usage of RNG k-ε turbulence model seems to be more efficient in this study is the general running time. According to numbers provided in Table 6 and previous sections, for two 2D simulations and two 3D simulations, totally, the difference in running time of RNG k-ε and SST k-ω turbulence models is approximately 536 hours (for 2D cases 18 hours and for 3D cases 250 hours). This increase in running time besides other technical info can be a good reason for the usage of RNG k-ε turbulence mode as the main model in this study.

6. Conclusion

The aim of this study was to investigate the aerodynamic performance of a doubled-row H-Darrieus VAWT in two different geometric configurations. For this purpose, first, an

ordinary H-Darrieus VAWT was simulated and verified based on a previous work which was conducted using BEM theory. The sliding mesh model besides RNG k-ε turbulence model resulted in a mean error of less than 7.4 % for two different cases which is acceptable in case of comparison between numerical and analytical approaches.

Introducing Doubled-Row H-Rotor Darrieus VAWT, this study was to calculate the amount of improvement of C_m when a second row with the same blade characteristics of the first row is added to an ordinary H-Darrieus VAWT. Two different doubled-row cases were simulated in this study. First was aligned case in which the second row was added aligned with the first row and second was non-aligned case in which rows had 60 degrees angular offset. Results showed that for an ordinary 3-bladed H-Darrieus VAWT with a radius of 1.5 meters; when a second row is added by radius of 1.7 meters with or without 60 degrees of angular offset, for inlet velocity of 8 m/s and TSR 4, C_m will be improved by about 314% which is very impressive in comparison with other ways of performance improvement.

All achieved results in this work were finally backed up by several supporting studies in which different criteria (turbulence model, geometry, solution methods) were changed and the effect of each of those was analyzed. It was observed that changing the turbulence model from RNG k-ε to SST k-ω increases the running time of about 25% while the difference in results is little (18%). Also, consideration of central shaft with a diameter of 0.2 to 0.5 m is able to change the results from 10 to 28%.

References

[1] P. I., "Double-Multiple Streamtube Model for Studying VAWT's," J. Propuls. Power, vol. 4, no. 4, pp. 370–378, 1988.

[2] T. G. Abu-el-yazied, H. N. Doghiem, and A. M. Ali, "Investigation of the Aerodynamic Performance of Darrieus Vertical Axis Wind Turbine," IOSR J. Eng., vol. 4, no. 5, pp. 18–29, 2014.

[3] M. Element and A. Blades, "ICFD11-EG-4039 Multi Element Airfoil Blades," pp. 1–9, 2013.

[4] K. Hamada, T. Smith, and N. Durrani, "Unsteady flow simulation and dynamic stall around vertical axis wind turbine blades," 46th AIAA Aerospaces …, no. January, pp. 1–11, 2008.

[5] L. X. Z. Y. B. Liang, X. H. L. Q. F. Jiao, and J. Guo, "Aerodynamic Performance Prediction of Straight-bladed Vertical Axis Wind Turbine Based on CFD," Adv. Mech. Eng., vol. 2013, p. 905379, 2012.

[6] Y. Chen and Y. Lian, "Numerical investigation of vortex dynamics in an H-rotor vertical axis wind turbine," Eng. Appl. Comput. Fluid Mech., vol. 9, no. 1, pp. 21–32, 2015.

[7] M. R. Hasan, R. Islam, G. M. H. Shahariar, and M. Mashud, "Numerical Analysis of Vertical Axis Wind Turbine," 9th Int. Forum Strategic Tech. (IFOST) pp. 318-321, 2014.

[8] H. F. Lam and H. Y. Peng, "Study of wake characteristics of a vertical axis wind turbine by two- and three-dimensional computational fluid dynamics simulations," Renew. Energy, vol. 90, pp. 386–398, 2016.

[9] M. Tahani, N. Babayan, S. Mehrnia, and M. Shadmehri, "A novel heuristic method for optimization of straight blade vertical axis wind turbine," Energy Convers. Manag., vol. 127, pp. 461–476, 2016.

[10] Y. Wang, X. Sun, X. Dong, B. Zhu, D. Huang, and Z. Zheng, "Numerical investigation on aerodynamic performance of a novel vertical axis wind turbine with adaptive blades," Energy Convers. Manag., vol. 108, pp. 275–286, 2016.

[11] J. H. Lee, Y. T. Lee, and H. C. Lim, "Effect of twist angle on the performance of Savonius wind turbine," Renew. Energy, vol. 89, pp. 231–244, 2016.

[12] Y. Li, Y. F. Zheng, F. Feng, Q. B. He, and N. X. Wang, "Numerical simulation on a straight-bladed vertical axis wind turbine with auxiliary blade," IOP Conf. Ser. Earth Environ. Sci., vol. 40, p. 12062, 2016.

[13] K. Rogowski, M. O. L. Hansen, R. Maroński, and P. Lichota, "Scale Adaptive Simulation Model for the Darrieus Wind Turbine," J. Phys. Conf. Ser., vol. 753, p. 22050, 2016.
[14] M. Scungio, F. Arpino, V. Focanti, M. Profili, and M. Rotondi, "Wind tunnel testing of scaled models of a newly developed Darrieus-style vertical axis wind turbine with auxiliary straight blades," Energy Convers. Manag., vol. 130, pp. 60–70, 2016.
[15] D. Saeidi, A. Sedaghat, P. Alamdari, and A. A. Alemrajabi, "Aerodynamic design and economical evaluation of site specific small vertical axis wind turbines," Appl. Energy, vol. 101, pp. 765–775, 2013.
[16] H. Dai, Z. Yang, and L. Song, "-w \ Fhght path," no. 71071078, pp. 695–700, 2014.
[17] N. Durrani, H. Hameed, H. Rahman, and S. R. Chaudhry, "A detailed Aerodynamic Design and analysis of a 2D vertical axis wind turbine using sliding mesh in CFD," 49th AIAA Aerosp. Sci. Meet. Incl. New Horizons Forum Aerosp. Expo., no. January, pp. 1–16, 2011.
[18] Y. T. Lee and H. C. Lim, "Numerical study of the aerodynamic performance of a 500W Darrieus-type vertical-axis wind turbine," Renew. Energy, vol. 83, pp. 407–415, 2015.
[19] O. Power, W. Meter, R. Dewil, L. Appels, and J. Baeyens, "User's Guide," Options, vol. 47, no. January, pp. 1711–1722, 2006.
[20] M. H. Shojaeefard, M. Tahani, M. B. Ehghaghi, M. A. Fallahian, and M. Beglari, "Numerical study of the effects of some geometric characteristics of a centrifugal pump impeller that pumps a viscous fluid," Comput. Fluids, vol. 60, pp. 61–70, 2012.
[21] B. Diskin and J. L. Thomas, "Comparison of Node-Centered and Cell-Centered Unstructured Finite Volume Discretizations: Inviscid Fluxes," Aiaa J., vol. 49, no. 4, pp. 836–854, 2011.
[22] ANSYS, "Introduction to ANSYS Fluent," ANSYS Cust. Train. Mater., no. December, pp. 1–59, 2010.
[23] T. J. Baker, "Mesh generation: Art or science?," Prog. Aerosp. Sci., vol. 41, no. 1, pp. 29–63, 2005.
[24] H. Lewyt, "Courant-Friedrichs-Lewy," no. March, 1967.
[25] F. D. I. Ingegneria, "Effect of Shaft Diameter on Darrieus Wind Turbine," 2013.